Mechanistic Study on the Continuous Flow Electrocoagulation of Silica Nanoparticles from Polishing Wastewater

Walter Den*

Department of Environmental Science and Engineering, Tunghai University, Taichung-Kan Road, Sec. 3 #181, Taichung, Taiwan 407, Republic of China

Chihpin Huang and Hung-Chieh Ke

Graduate Institute of Environmental Engineering, National Chiao Tung University, Po-Ai Street #75, Hsinchu, Taiwan 300, Republic of China

This study investigates the removal mechanisms involved in the monopolar, continuous-flow electrocoagulation of a polishing wastewater containing negatively charged silica particles. Using iron as the anodes, the mechanisms were inferred from the experimental observations of the changes in pH, zeta-potential, and turbidity as a function of reaction time, as well as from the sludge characterization. Two types of distinct mechanisms were observed, one involving particle destabilization by oppositely charged ferrous ions and the other involving coprecipitation or enmeshment of silica particles with the iron hydroxides. The former mechanism was apparently responsible for the formation of "surface flocs", whereas the latter one was responsible for the "sediment sludge". The sludge collected separately from the two "sinks" was distinctly different in both physical appearance and settling velocity. Furthermore, based on the sheer quantity of the surface flocs and the sediment sludge, the two mechanisms involved in the electrocoagulation process were equally important to the silica removal.

Introduction

In the past 10 years, electrochemical processes have received renewed interest as an alternative treatment method for industrial wastewater containing dispersed charged particles without chemical additions. For instance, the performance and feasibility of electrocoagulation and electroflotation processes was demonstrated for treating wastewater generated from restaurant,[1] textile,[2,3] and silicon wafer polishing processes.[4−6] The future prospect of the technology was also meticulously discussed by Holt and co-workers,[7] detailing the suitable fields of application for the relevant electrochemical processes operated under different modes (batch or continuous flow) and parametric conditions (current density and bubble density). In principle, electrocoagulation plays the central role among other electrochemical processes that also include electroflotation and electrodecantation. In this process, the sacrificial anodic electrodes (e.g., iron and aluminum) are used to continuously supply metallic ions as the source of coagulants. These electrochemically generated metallic ions can hydrolyze near the anode to form a series of metallic hydroxides capable of destabilizing dispersed particles. The simultaneous electrophoretic migration of the negatively charged particles (e.g., silica particles) toward the anode forces chemical coagulation between particles and metallic hydroxides in the vicinity of the anode, forming flocs that either settle or redeposit onto the anode.

Numerous studies specifically targeting electrocoagulation of ultrafine particles have been reported.[8−10] For example, Matteson et al.[8] described that the aggregation and removal process of a kaolin particle followed second-order kinetics, on the basis of which a mathematical model for batch and continuous-flow electrocoagulation was developed. Holt et al.[9] differentiated the mechanisms between chemical coagulation and electrocoagulation using aluminum as the coagulant for the removal of clay particles. Canizares et al.,[10] in turn, discussed the possible electrocoagulation mechanisms of kaolin particles based primarily on the correlation between the time-dependent change of turbidity and the corresponding aluminum concentration. In addition, Mollah et al.[3] employed a continuous-flow, bipolar reactor with iron electrodes to treat dye particles. They proposed that chemical coagulation involving several iron oxides was responsible for the dye removal on the basis of the X-ray diffractometric analysis of the residue.

Despite the contribution of the aforementioned studies that enhanced our understanding of the electrocoagulation process, hardly any consensus could be drawn, especially if one considers the wide variation between the properties of water samples (e.g., pH, conductivity, surface charge, etc.). The present study, therefore, intends to focus on investigating the mechanisms and their relative contributions in the electrocoagulation of chemical-mechanical planarization (CMP) wastewater, one of the most notable industrial wastewaters containing highly charged ultrafine particles. The nature of the wastewater, as well as the parameter optimization and process kinetics of electrocoagulation, was reported in our previous studies using a channelized continuous-flow reactor with monopolar iron electrodes.[6,11] In brief, the CMP process for silicon-oxide planarization typically generates wastewater containing very dilute fumed silica particles that are narrowly ranged between 50 and 200 nm. These particles possess strong negative surface charges that repel the adjacent ones when they are immersed in base solutions. As a result, the highly homogeneous characteristics of the CMP wastewater render it an ideal industrial effluent for studies involving electrocoagulation.

Materials and Methods

CMP Wastewater. The CMP wastewater used throughout this study was obtained from a full-scale semiconductor

* To whom correspondence should be addressed. Tel.: +886-4-23590121 ext 3050. Fax: +886-4-23594276. E-mail: wden@thu.edu.tw.

10.1021/ie0514410 CCC: $33.50
Published on Web 04/19/2006

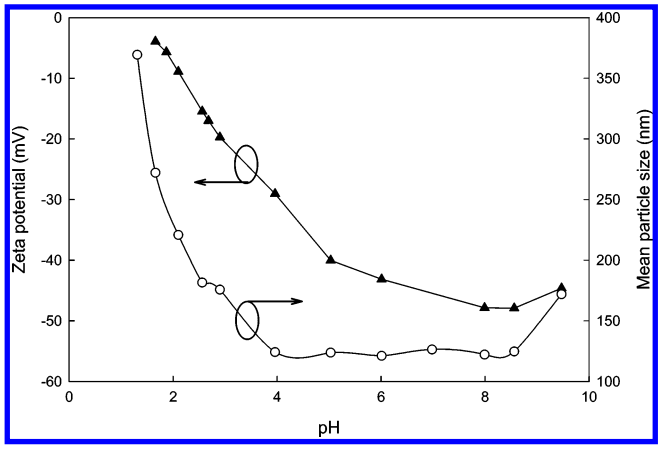

Figure 1. Zeta-potential and mean particle size as a function of wastewater pH.

manufacturing plant in the Science Industrial Park in Hsinchu, Taiwan. The "oxide" CMP wastewater, which was segregated from other sources of processing wastewater, is typically characterized with turbidity in the range between 150 and 450 NTU, conductivity between 100 and 150 μS/cm, and pH between 7.5 and 9.0. The size and distribution of the particles in the CMP wastewater were measured by a Malvern particle analyzer (Mastersizer 2000, Malvern Instruments, U.K.), and the surface potential of the particles was measured by a zeta (ζ)-potential analyzer (ZetaPlus, Brookhaven Instruments, U.S.A.). A representative set of particle characteristics with respect to ζ-potential and particle size as a function of wastewater pH is shown in Figure 1. The isoelectric point of the wastewater was below pH 2, with the corresponding mean particle size approaching 400 nm. Furthermore, the particle size appears to stabilize ($\sim$110 nm) at pH > 4, suggesting that particle collision energy was sufficient to overcome the electrical repulsive force for ζ-potential < -30 mV, leading to particle agglomeration and rapid size growth. For the CMP wastewater, the silica concentration and turbidity formed a well-behaved linear correlation within the concentration range, and thus, turbidity was employed as the representative parameter. In addition, the organic content of the wastewater, measured as total organic carbon (TOC) by a Shimadzu TOC analyzer (TOC-5000A) after filtering with 0.45 μm membranes, fluctuated between 10 and 60 mg L^{-1} during the study. The TOC concentration was found to be closely linked to the turbidity—and thus, to the silica concentration.

Experimental Methods

An 8-L continuous-flow reactor channelized by the electrode plates (20 cm × 14 cm) was used throughout the electrocoagulation study. The anodic plates (ASTM A36-97a iron) were completely submerged, and the cathodic plates (JIS SUS304 stainless steel) were partially submerged in the suspension. The electrode plates were interposed equidistantly to create vertical flow channels with uniform electrical field strength under monopolar electrical arrangement. A manually controllable DC power supply (Goodwill Instruments, Taiwan) was operated in constant-current mode (0−3 A), with the voltage response (0−200 V) monitored and recorded by a data-acquisition system. During the experiment, the wastewater was continuously delivered into the reactor using a microcomputer-controlled peristaltic pump (Masterflex L/S, Cole Parmer, IL) at various flow rates. Samples from the influent and effluent ports were routinely taken and measured for turbidity (Hach ratioTM/XR turbidity meter, U.S.A.), pH/conductivity (inoLab WTW pH meter), total residual iron concentration by inductively coupled plasma−atomic emission spectroscopy (ICP−AES, Jobin-Yzon JY24, France), and TOC. Also, after the effluent turbidity approached a stable level, the particle size and ζ-potential were analyzed as the wastewater flowed through each channel.

The current efficiency was determined through batch experiments with six pairs of electrodes in the laboratory-scale reactor. Instead of CMP wastewater, reverse osmosis (RO) water was used as the electrolyte medium to minimize iron consumption. After 10 min of electrolysis, the electrodes were removed from the reactor, and the aqueous medium was vigorously stirred before samples were taken for total iron analyses with ICP−AES. The current efficiency (ϵ_c) was defined as the ratio of the actual mass of iron ($[Fe]_R$) to the theoretical mass of iron ($[Fe]_T$) liberated from the anodes:

$$\epsilon_c = \frac{[Fe]_R}{[Fe]_T} \tag{1}$$

In eq 1, the theoretical mass of iron liberation is calculated from Faraday's law for a monopolar arrangement,

$$m_{Fe} = \frac{i\tau M_{W,Fe}}{ZF} \tag{2}$$

where i is denoted as the applied current (A), τ is the duration of electrolysis, Z is the valence number of in situ metal ions (=2 for Fe), F is the Faraday's constant (=96 500 C), and M_W is the molecular weight of Fe.

Sludge Characterization. To characterize the sludge property, the flocs attached on the anodic surfaces were scraped off as much as possible, and the sediments were collected from the reactor bottom after completion of a 2-h run. The wet and dry weights of the flocs and the sediments were individually measured, and their water contents were recorded after oven drying (105 °C). The sedimentation tests for the flocs and the sediments were performed using a 1-L glass column (40-cm calibrated height). The height of the solid/liquid interface was recorded over the course of the sedimentation. Subsequently, the settling velocity was determined by the slope of the linear correlation between the interface height and the settling time during the initial sedimentation period. The crystalline composition of the sludge was analyzed by an X-ray diffractometer (Shimadzu XRD-600, Japan).

Results and Discussion

Variation of Parameters during Electrocoagulation. (a) Dynamic Response of Turbidity, Iron Concentration, pH, and Conductivity. An appropriate range of the operating conditions, specifically the hydraulic retention time (30−100 min) and the applied current density (4−7 A m^{-2}), has been previously established using the identical system.[6,11] A typical set of dynamic-response profiles for the effluent turbidity and iron concentration, along with the effluent pH and conductivity, are shown in parts a and b of Figure 2, respectively. The turbidity-response profile indicates that an initial increase in the effluent turbidity was normally experienced, followed by a rapid reduction before reaching a near steady-state condition after 100 min of treatment. The corresponding effluent iron concentration profile also exhibited a peak value after 20 min. The initial increase in both turbidity and iron concentration was because, at the commencement of electrolysis, the particles and the iron species liberated from the anodes closer to the reactor effluent

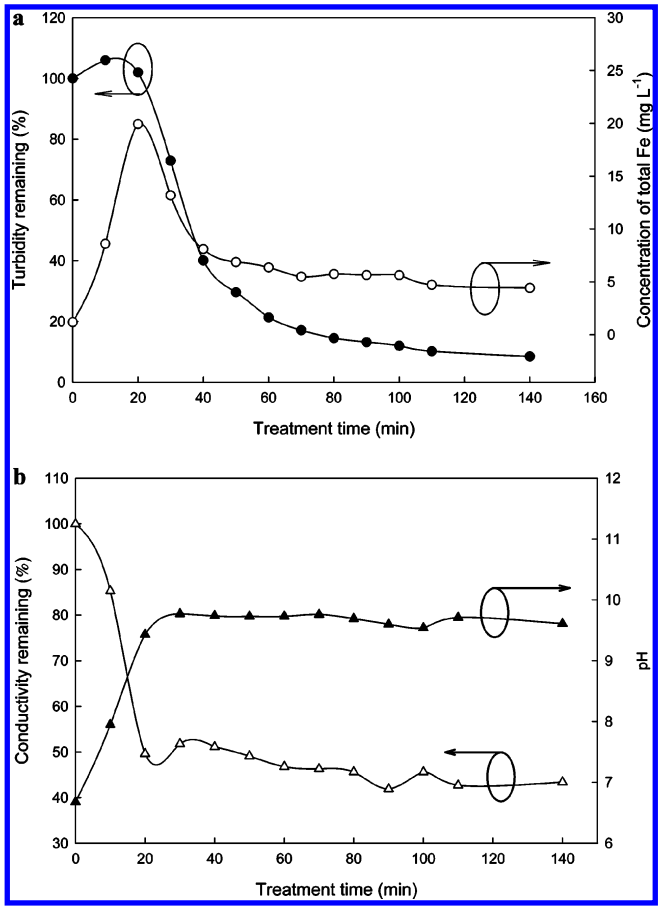

Figure 2. Time-varying effluent profiles of (a) fraction of turbidity removal and total Fe concentration and (b) fraction of conductivity removal and pH. Initial turbidity = 200 NTU, initial conductivity = 113 μS/cm, current density = 5.71 A/m^2, and retention time = 100 min.

did not have sufficient time to undergo coagulation effectively before exiting the reactor. However, as the process progressed, a period of rapid reduction in both turbidity and iron concentration can be observed, indicating that the ferrous ions and their hydroxyl species were effectively consumed during particle coagulation. One can also observe that the residual turbidity continued to decline, albeit very gradually, even though the iron concentration appeared to stabilize after 60 min of operation. This result could be explained by the continual agglomeration of the flocs that eventual settled out from the wastewater, hence reducing the turbidity by further taking up ferrous coagulants. Furthermore, it is worth noting that, even as the system was operated under an optimum condition, a small fraction of residual turbidity (<5 NTU) would always remain in the effluent. Passing the treated effluent through a filter membrane, however, would significantly reduce the turbidity, suggesting that the residual effluent turbidity was not caused by the silica particles alone but rather by larger flocs that most probably consist of precipitates (i.e., iron hydroxide) from the electrolysis of anodes.

As shown in Figure 2b, the conductivity in the effluent sharply decreased with time before stabilizing at a residual value of roughly 50% of the influent conductivity. In contrast, the pH of the effluent initially rose and approached a stable alkaline pH of ~9.5, forming almost a mirror image to the conductivity profile. The removal of conductivity, which bears importance in yielding greater potential across each channel with a fixed current density, was likely a consequence of the electrochemical reduction of potassium ions, which represents a major source of conductivity from dilute potassium hydroxide (KOH) commonly used as an alkaline dispersant in commercial polishing slurries. The existence of potassium in the wastewater was confirmed, though not further quantified, through the energy-dispersive X-ray (EDX) examination of the raw wastewater samples. Moreover, as reported in many other electrocoagulation studies for water/wastewater treatment, this equilibrium pH was an event of dynamic balance between the complex chemical reactions involving a H^+ or OH^- donor and acceptor during electrocoagulation. The outcome of the stable alkaline pH can be best described by the dynamically predominant cathodic water reduction (eq 3) over anodic water oxidation (eq 4) and iron hydroxylation (eqs 5 and 6):

$$2H_2O + 2e^- \rightarrow 2OH^- + H_{2(g)} \quad (3)$$

$$2H_2O \rightarrow O_{2(g)} + 4H^+ + 4e^- \quad (4)$$

$$Fe^{2+}_{(aq)} + 2\ OH^- \rightarrow Fe(OH)_{2(s)} \quad (5)$$

$$Fe^{3+}_{(aq)} + 3\ OH^- \rightarrow Fe(OH)_{3(s)} \quad (6)$$

The role of eqs 3 and 4 will be further discussed in this article.

(b) Particle-Size Evolution. In the continuous-flow electrocoagulation process, one would anticipate a growth of particle size if coagulation occurs. To facilitate this observation, upon reaching a steady-state condition (i.e., effluent turbidity no longer changing with treatment time), the average particle size of the samples collected from each flow channel was determined, and the results grouped into four distinct downstream zones are shown in Figure 3. One can observe that, within zone I, the particle size and distribution remain essentially unchanged, having a normal distribution with mean particle size nearly identical to that of the untreated CMP wastewater (~110 nm). When reaching zone II, particle coagulation commences and flocs are formed; hence, the mean particle size became larger and the distributions were typically broadened and skewed. The turbidity of the wastewater samples from this zone usually experiences a temporary rise, most probably because of the presence of the suspending flocs. Zone III is characterized by size distribution with bimodal peaks, showing the decreasing quantity of small particles and the progressive increase in the quantity of flocs > 1 μm. The wastewater turbidity in this zone reduces rapidly as a result of floc settling and deposition onto the anodic surfaces. Finally, it could be noted that the size distributions in zone IV, while still broad and rather random, appear to reapproach a normal distribution with mean particle size in the proximity of 600 nm. The fractions of particle size at both extremes of the distribution profiles were substantially reduced from the previous zones, suggesting that the majority of small particles are coagulated and large flocs are removed by either settling or deposition. This latter result also supports the previous interpretation on the cause of the residual turbidity in the effluent. Furthermore, these observations are consistent with a study reported by Holt et al.,[9] in which the aluminum-based electrocoagulation was performed for the removal of clay particles. In that study, the investigators categorized the process into three distinct "stages" according to the change of turbidity as a function of electrocoagulation time, namely, the lag stage, the reactive stage, and the stabilizing stage. Hence, using the particle-size distribution as the direct evidence, the successive electrocoagulation process could also be described in the four phenomenological zones.

(c) Current Efficiency. Figure 4 shows the variation of the total iron concentration and the corresponding current efficiency

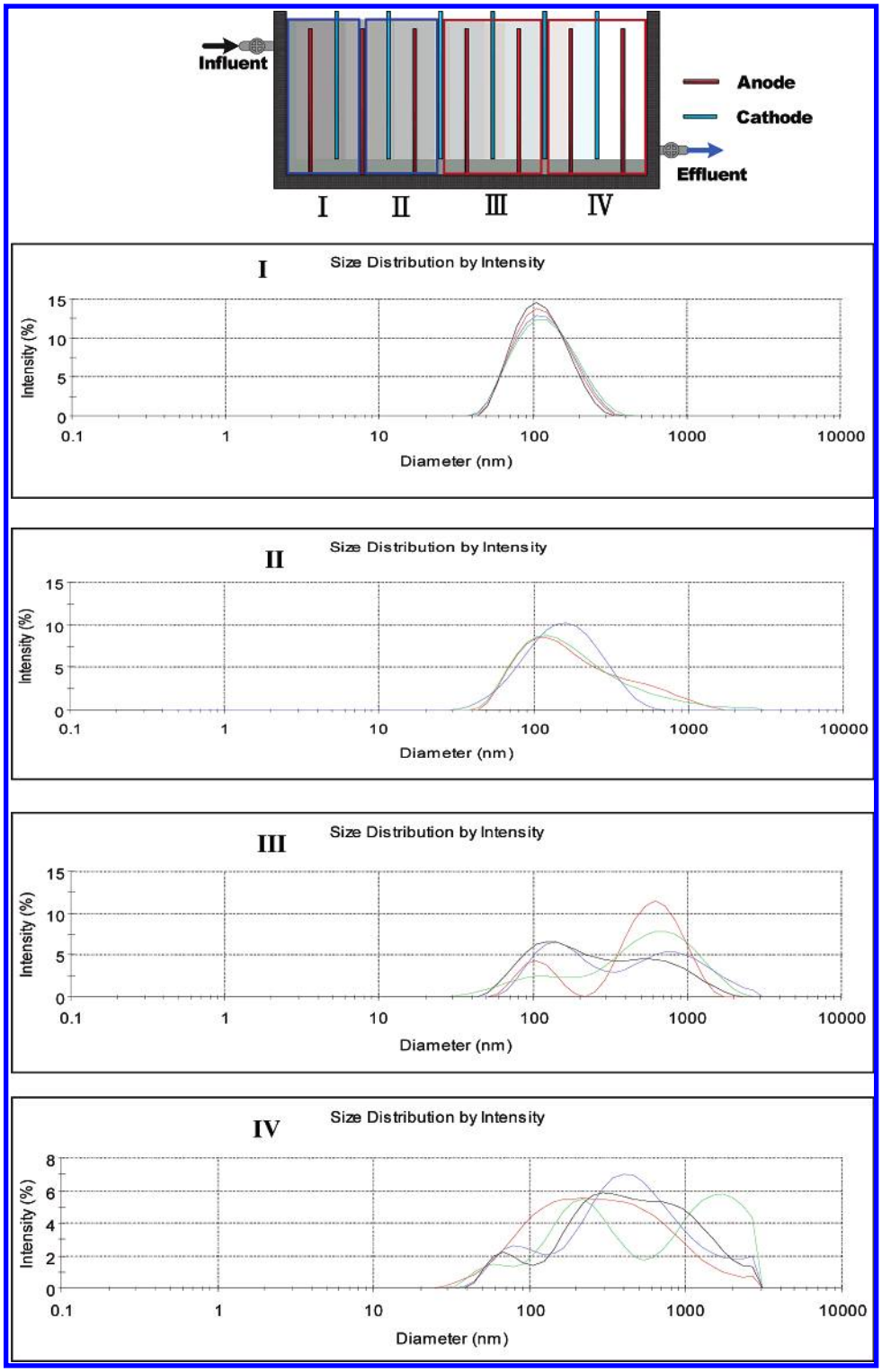

Figure 3. Change of particle-size distribution profiles in the four successive zones of the electrocoagulation reactor as indicated in the top of the figure.

as a function of the applied current density in the batch electrolysis study with RO water. To relate these parameters with the actual electrocoagulation performance, the steady-state turbidity removal efficiency obtained under different current densities was also composited in the same figure. Evidently, this monopolar electrocoagulation process operated with low current efficiencies, as the total iron concentration only slightly increased as the applied current density was elevated from 1.4 to 5.7 A/m^2. This was because the passivated iron anodic surfaces entailed a critical current to initiate a breakdown of the passivating film or to create numerous surface defects such that liberation of ferrous ions could be facilitated, as occurred when current density was >5.7 A/m^2. The observed low current efficiency could be further substantiated by comparing the actual cell potentials with the ohmic potentials during electrocoagulation. In this study, the actual cell potential was directly recorded from the voltage indicator after at least 60 min of operation (i.e., near steady state with respect to residual turbidity and conductivity), and the ohmic potential ($d/\kappa j$) was calculated based on the applied current density (j), the interelectrode distance (d), and the corresponding residual conductivity (κ). As shown in Figure 5, a significant difference between the actual

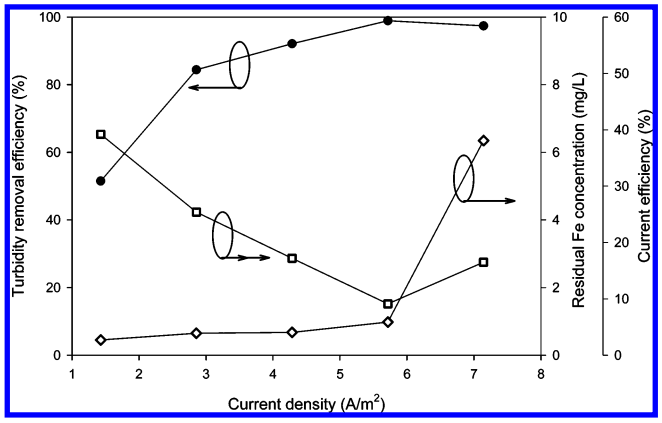

Figure 4. Effect of current density on the steady-state turbidity removal efficiency (●), current efficiency (□), and the total residual iron concentration (◇).

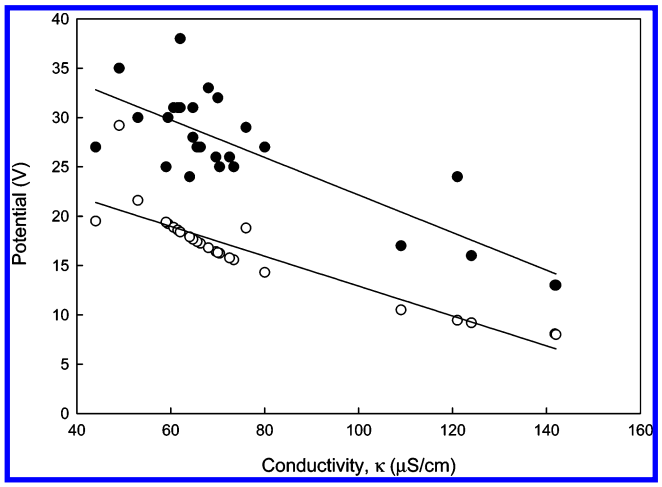

Figure 5. Measured overpotential (●) and the calculated ohmic potential (○) as a function of aqueous conductivity.

cell potentials and the ohmic potentials was observed for samples with κ ranging between 40 and 140 μS/cm. As illustrated by Chen et al.,[12] the overpotential due to an anodic passive film could significantly increase the intensity of the electrical current passing through an electrochemical reactor. Yet, it was interesting to note that the best turbidity removal efficiency occurred at a current density of 5.7 A/m^2, at which point the lowest current efficiency was also experienced. This result suggests that, for the range of silica concentrations investigated in this study, the current efficiency is inconsequential to the performance of electrocoagulation, insofar as a sufficient amount of ferrous ions electrochemically released from the anodes is available. In fact, deterioration of system performance with respect to turbidity removal efficiency was usually accompanied by the abrupt increase of total iron concentration in the effluent, as reported in the previous studies.[6]

Role of ζ-Potential in the Electrocoagulation Process. Considering that the effluent pH always approached 9.5 regardless of the operating conditions during electrocoagulation, coupled with the observation of the change of particle size along the continuous-flow reactor, it becomes motivating to examine the change of ζ-potential during the course of the process. Figure 6a shows the time-history of the ζ-potential profiles for CMP wastewater samples taken from the bulk liquid and from near the anodic surface during electrocoagulation. It can be observed that, after 30 min, the ζ-potential of the bulk wastewater gradually approached a stable value of −35 mV. The samples taken from near the surface, however, exhibited a very different

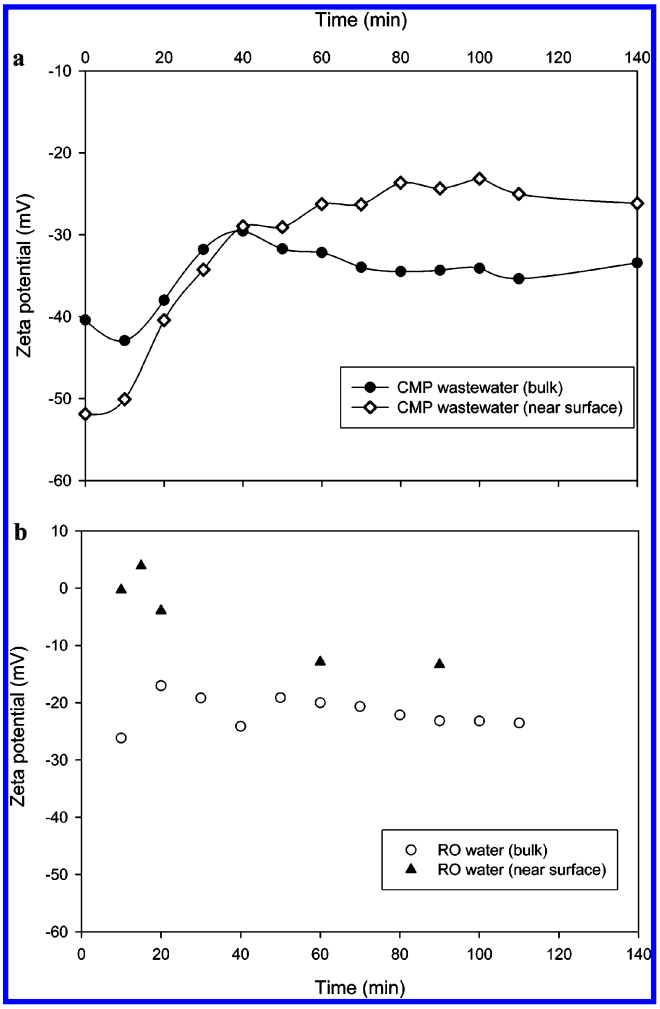

Figure 6. Comparison of the ζ-potentials between electrocoagulation samples: (a) CMP wastewater from bulk wastewater (●) and wastewater near anodes (◇); and (b) RO water from bulk (○) and near surface (▲).

ζ-potential pattern, starting with a more negative potential (−50 mV) and stabilizing at a less negative potential (−25 mV) than the bulk wastewater. To help elucidate this difference, the ζ-potential profiles for the electrocoagulation of RO water were also established, as shown in Figure 6b, such that the variability caused by the silica particles in the CMP wastewater could be eliminated. Clearly, the steady ζ-potential for the iron hydroxyl species displayed in Figure 6b was in the vicinity of −20 mV, with a stabilized pH of 9.2. As assessed from these data, the highly negative value of the near-surface ζ-potential for the CMP wastewater shortly after commencement of electrocoagulation could be ascribed to the dense silica particles that electrophoretically migrated near the anodic surfaces. Conversely, the lesser value of ζ-potential at steady state was primarily contributed from the iron hydroxyl species. The ζ-potential profile of the bulk liquid, in turn, appears to average out that of the near-surface samples, because the charged iron hydroxyl species eventually diffused away from the surfaces. It should also be noted in Figure 6b that the initial ζ-potential of the iron species were either positively charged or uncharged (net) near the anodic surfaces. This result implies the release of ferrous ions that gradually transformed into negatively charged hydroxyl or hydroxide species.

Examination of the Pourbaix diagram imparts that the iron hydroxyl species under alkaline and well-aerated conditions are predominantly $Fe(OH)_3$ and $Fe(OH)_4^-$. This was also attested in Figure 7, which illustrates that both silica particles and the

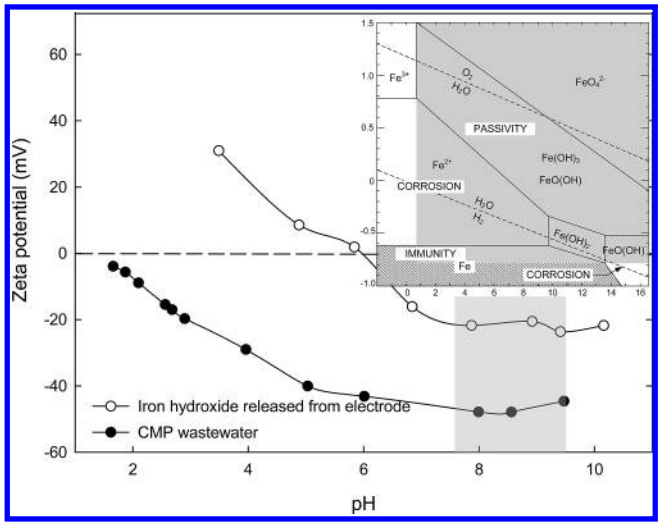

Figure 7. ζ-potential profiles as a function of pH for the CMP wastewater (●) and the electrolyzed RO water (○). The shaded area indicates the range of pH of the CMP wastewater, and the inset shows the Pourbaix diagram of iron (10^{-6} M) for reference for the discussion in the text.

aged iron hydroxides are negatively charged within the typical pH range of oxide CMP wastewater (shaded area). Obviously, these hydroxyl species carrying neutral or negative charges cannot proceed charge neutralization with the negatively charged silica particles, and thus, coagulation via charge neutralization was improbable. Jar tests (rapid mixing at 200 rpm for 1 min, slow mixing at 30 rpm for 20 min, and settling for 30 min) using the aged solution obtained from the RO electrocoagulation also showed no evidence of coagulation with the CMP wastewater as well as no significant change in ζ-potential. These results provide direct evidence of a particle-removal mechanism by coprecipitation (or enmeshment) between silica particles and iron hydroxides, which typically forms a suspended gel capable of binding colloids or particles previously observed in other studies.[3] It is also worth noting that the TOC in the CMP wastewater was partially removed during the electrocoagulation process. As mentioned previously, the wastewater TOC was strongly correlated to its turbidity, suggesting that the TOC came primarily from the organic additives of the polishing slurries (as dispersion stabilizing agents that create metastable homogeneous suspensions). Therefore, the reduction in TOC was more likely due to the removal of particles than due to the direct organic oxidation.

On the basis of the experimental results presented above, two major possible mechanisms, namely, charge neutralization and coprecipitation, are operative in the electrocoagulation process. A conceptual view of this process is schematized in Figure 8, providing a systematic way to describe these mechanisms:

(*i*). When the applied potential is adequate such that the kinetic and anodic passive overpotential can be compensated to sufficiently liberate Fe^{2+} from the iron anodes, these ferrous ions immediately participate in charge neutralization with the silica particles already migrated to the vicinity of the anodic surfaces (eq 7). This directly leads to particle destabilization and, subsequently, coagulation, forming flocs that mostly redeposit onto the pits of the anodic surfaces through electrostatic attraction (eq 8).

$$Fe_{(s)} \rightarrow Fe^{2+}_{(aq)} + 2e^- \quad (7)$$

$$Fe^{2+}_{(aq)} + SiO^- (\text{silica}) \rightarrow \text{floc } (\downarrow) \quad (8)$$

These greenish deposits, which are characteristic of the Fe^{2+} or its hydroxyl species, would eventually turn yellowish due to oxidation of the ferrous species. This mechanism is primarily responsible for the "surface flocs".

(*ii*) The Fe^{2+} that do not participate in direct charge neutralization with the silica particles slowly diffuse outward into the bulk liquid and form various iron hydroxyl species. Additionally, in liquid with sufficiently high dissolved oxygen concentration, the ferrous ions are oxidized to ferric ions (eq 11b) and thereby the formation of both ferrous and ferric hydroxyl species are possible. If these hydroxyl species are not consumed in charge neutralization, then the stable hydroxides will form as the end products (eqs 11a and 11c).

$$Fe_{(s)} \rightarrow Fe^{2+}_{(aq)} + 2e^- \quad (9)$$

$$2H_2O + 2e^- \rightarrow 2OH^- + H_{2(g)} \quad (10)$$

$$Fe^{2+}_{(aq)} + 2\,OH^- \rightarrow Fe(OH)_{2(s)} \quad (11a)$$

$$Fe^{2+}_{(aq)} + 4H^+ + O_2 \rightarrow Fe^{3+} + 2H_2O \quad (11b)$$

$$Fe^{3+}_{(aq)} + 3\,OH^- \rightarrow Fe(OH)_{3(s)} \quad (11c)$$

Under high pH and oxygenated conditions, the ferrous ions and their hydroxyl species can also easily form $Fe(OH)_3$ and α-FeOOH (goethite) as coproducts (eq 12). They may further react to form hydrogenated iron hydroxyl species, which can bound or enmesh with the silica particles to become flocs that precipitate to the bottom of each cell (eqs 13 and 14).

$$Fe(OH)_{2(s)} + H_2O + O_2 \rightarrow Fe(OH)_{3(s)} + \alpha\text{-}FeOOH_{(s)} \quad (12)$$

$$Fe(OH)_{3(s)} + \alpha\text{-}FeOOH_{(s)} \rightarrow H_{(aq)}(OH)OFe_{(s)} \quad (13)$$

$$H_{(aq)}(OH)OFe_{(s)} + SiO^- (\text{silica}) \rightarrow \text{floc } (\downarrow) + H_2O \quad (14)$$

It is noted that both α-FeOOH and FeO(OH) have been identified by the XRD analysis, a typical sample of which is shown in Figure 9. In addition, a variety of iron oxides (Fe_2O_3, $Fe_{21.3}O_{32}$, etc.) and silicon oxide were also observed. None of the crystalline, however, showed an Fe−Si composite, hence confirming that silica particles are removed strictly by coagulation (i.e., no chemical reaction forming Fe−Si bonding). The flocs formed from the coprecipitation mechanism eventually settled to the floor of the reactor, thereby producing the "sediment sludge".

Sludge Characterizations. Considering that the two sinks of the electrocoagulation process, namely, the "surface flocs" and the "sediment sludge", are attributed to two distinct mechanisms, one would expect a difference in the physical properties of the sludge. Therefore, after each 2-h continuous-flow electrocoagulation experiment, the surface flocs were scraped off from the anodic plates and the sludge was collected from the reactor floor in separate efforts. In general, the sludge concentration (∼7800 mg/L) and sludge volume (∼150 mL) of the surface flocs were both greater than those of the sediment sludge (∼5000 mg/L and ∼100 mL). Even though the ratio of sludge volume between the surface flocs and the sediment sludge may change as the electrocoagulation process proceeds longer due to, for instance, the gradual saturation of the surface deposition site, these results corroborate that both removal mechanisms (i.e., charge neutralization and coprecipitation) were equally important in the electrocoagulation process. Furthermore, the settling curves of the two types of sludge shown in Figure

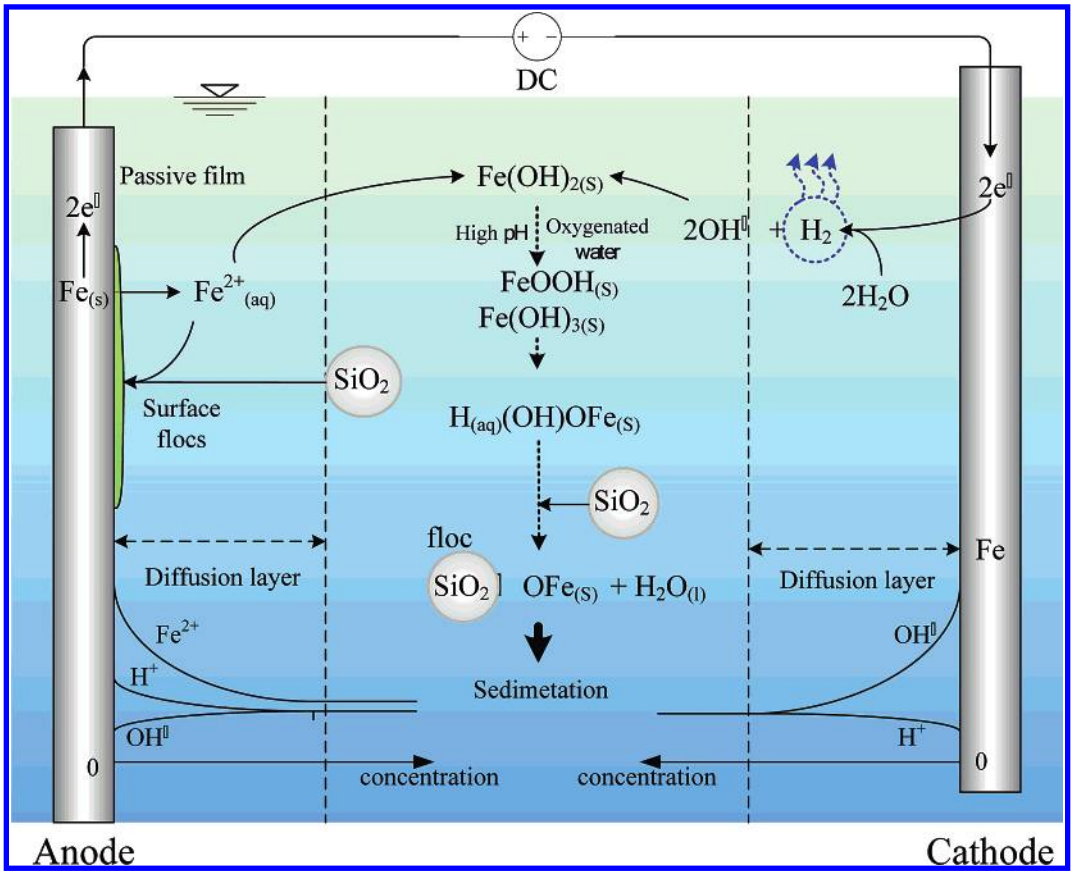

Figure 8. Conceptual view of the possible electrocoagulation mechanisms involved in the removal of silica colloids from wastewater with iron anodes. The diffusion layers have been exaggerated to illustrate their existence.

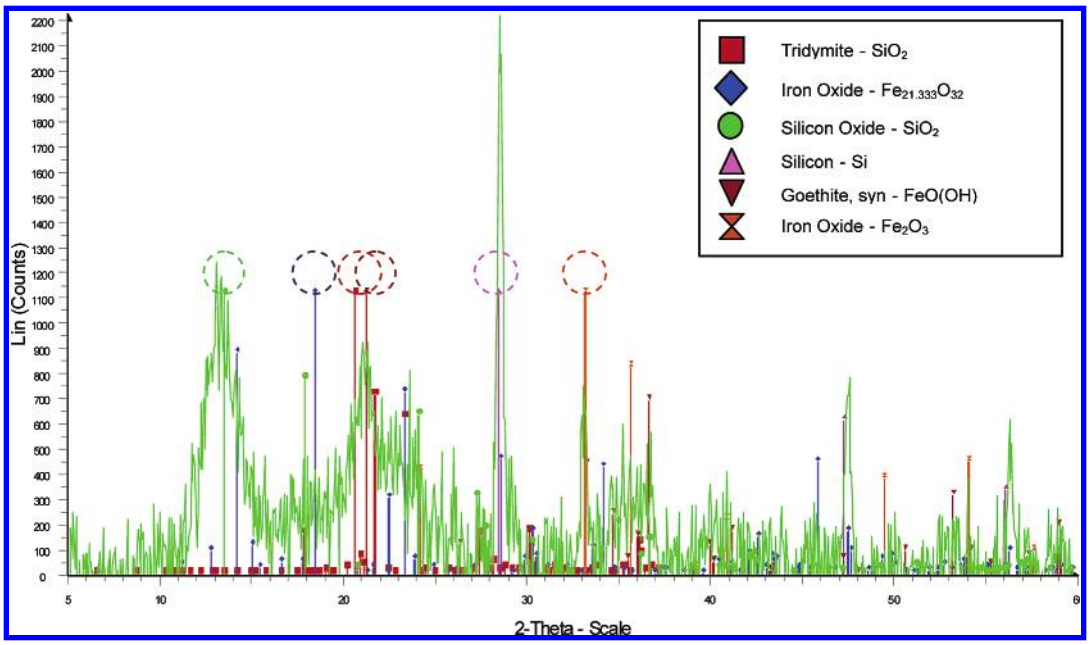

Figure 9. X-ray diffractometry for the typical sludge sample.

10a both exhibited a clear sequence of zone settling, transition settling, and compression settling. The settling velocities derived from the zone-settling regions indicated a faster settling of the sediment sludge (2.0 cm/min) than the surface flocs (0.57 cm/min). However, as sketched in Figure 10b, the effect of compression settling for the surface flocs was much more apparent than that for the sediment sludge, whose supernatant remained somewhat milky even after several hours of sedimentation. This observation could be best explained by recognizing that a small fraction of the sediment could consist of dense silica particles that were not coprecipitated but rather were self-settled by the effect of electrodecantation.[4]

Conclusions

This study investigated the removal mechanisms involved in the electrocoagulation of silica particles from CMP wastewater in a continuous-flow reactor featuring channelized cells and iron

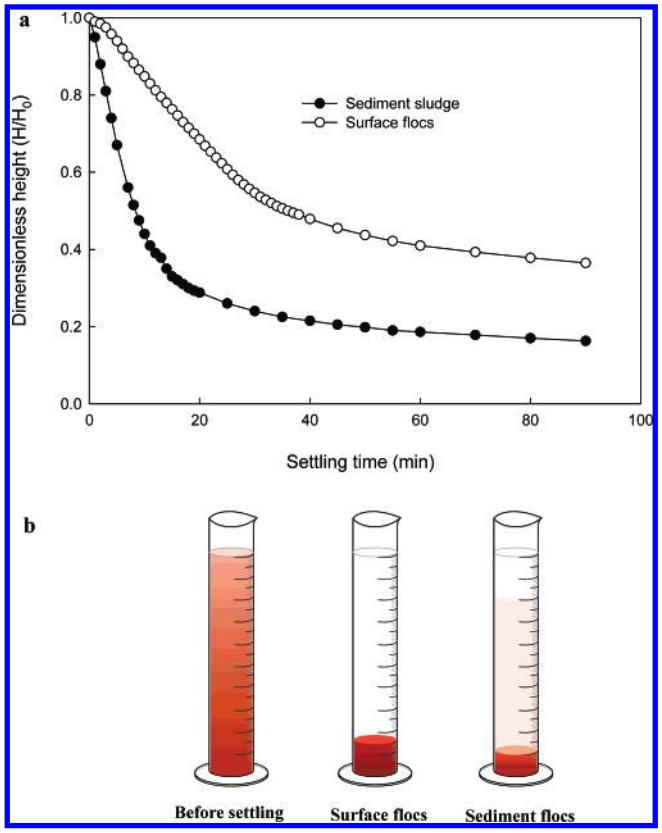

Figure 10. (a) Settling curves and (b) schematics of settling results for the surface flocs and the sediment sludge.

anodes with monopolar arrangement. Direct evidence of particle-size evolution along the length of the reactor was presented, showing distinct zones in which the particle-size distribution changed from near-normal to bimodal distribution, then reapproached normal distribution with a larger mean particle size. In addition, the investigators also found that, for a continuous-flow monopolar system, current efficiency was not a significant factor to the particle removal efficiency, although there appeared to be an optimal range of iron concentration associated with the removal efficiency.

ζ-potential measurement helped elucidate the particle removal mechanisms. Comparison between the time-dependent ζ-potential profiles for samples taken from the bulk wastewater and from near the anodic plates, as well as those from the RO water during electrocoagulation, suggested that particle destabilization via charge neutralization only occurred near the surface of the anodic plates. The remaining ferrous ions quickly transformed into iron hydroxides or hydroxyl complexes as they diffused away from the anodic surface. Since charge neutralization was improbable by virtue of the negative charges carried by both silica particles and the aged iron hydroxides, silica-particle removal could only occur by coprecipitation with the iron species.

The characteristic distinction of the sludge generated from the two mechanisms was also studied. The surface flocs due to particle destabilization by charge neutralization exhibited a slower settling velocity but a clearer supernatant as compared to those of the sediment sludge, which was caused by coprecipitation. Both types of sludge were comparable in sludge concentration and volume after 2 h of continuous-flow electrocoagulation, indicating that both mechanisms were equally important to the removal of silica particles.

Literature Cited

(1) Chen, G.; Chen, X.; Yue, P. L. Electrocoagulation and Electroflotation of Restaurant Wastewater. *J. Environ. Eng.* **2000**, *126*, 858.

(2) Kobya, M.; Can, O. T.; Bayramoglu, M. Treatment of Textile Wastewaters by Electrocoagulation Using Iron and Aluminium Electrodes. *J. Hazard. Mater.* **2003**, *B100*, 163.

(3) Mollah, M. Y. A.; Pathak, S. R.; Patil, P. K.; Vayuvegula, M.; Agrawal, T. S.; Gomes, J. A. G.; Kesmez, M.; Cocke, D. L. Treatment of Orange Azo-Dye by Electrocoagulation (EC) Technique in a Continuous Flow Cell Using Sacrificial Iron Electrodes. *J. Hazard. Mater.* **2004**, *B109*, 165.

(4) Belongia, B. M.; Haworth, P. H.; Baygents, J. C.; Raghavan, S. Treatment of Alumina and Silica Chemical Mechanical Polishing Waste by Electrodecantation and Electrocoagulation. *J. Electrochem. Soc.* **1999**, *146*, 4124.

(5) Lai, C. L.; Lin, S. H. Treatment of Chemical Mechanical Polishing Wastewater by Electrocoagulation: System Performances and Sludge Settling Characteristics. *Chemosphere* **2004**, *54*, 235.

(6) Den, W.; Huang, C. P. Electrocoagulation for Removal of Silica Nano-Particle from Chemical-Mechanical-Planarization Wastewater. *Colloids Surf., A* **2005**, *254*, 81.

(7) Holt, P. K.; Barton, G. W.; Mitchell, C. A. The Future for Electrocoagulation as a Localized Water Treatment Technology. *Chemosphere* **2005**, *59*, 355.

(8) Matteson, M. J.; Dobson, R. L.; Glenn, R. W., Jr.; Kukunoor, N. S.; Waits, W. H., III; Clayfield, E. R. Electrocoagulation and Separation of Aqueous Suspensions of Ultrafine Particles. *Colloids Surf., A,* **1995**, *104*, 101.

(9) Holt, P. K.; Barton, G. W.; Wark, M.; Mitchell, C. A. A Quantitative Comparison between Chemical Dosing and Electrocoagulation. *Colloids Surf., A* **2002**, *211*, 233.

(10) Canizares, P.; Martinez, F.; Carmona M.; Lobato, J.; Rodrigo, M. A. Continuous Electrocoagulation of Synthetic Colloid-Polluted Wastes. *Ind. Eng. Chem. Res.* **2005**, *44*, 8171.

(11) Den, W.; Huang, C. P. Electrocoagulation of Silica Nano-Particles in Wafer Polishing Wastewater by a Multi-Channel Flow Reactor: A Kinetic Study. *J. Environ. Eng.* **2006**, paper in review.

(12) Chen, X.; Chen, G.; Yue, P. L. Investigation on the Electrolysis Voltage of Electrocoagulation. *Chem. Eng. Sci.* **2002**, *57*, 2449.

Received for review December 26, 2005
Revised manuscript received March 23, 2006
Accepted March 23, 2006

IE0514410